Microwave Review
July 2024, Vol. 30, No. 1, pp. 67-74
DOI: 10.18485/mtts_mr.2024.30.1.9

Design of Low Noise, High Dynamic Range and Triple-Band MMIC Voltage Variable Attenuator Using 0.25 μm GaAs pHEMT Technology

Subham Banerjee[1], Md Sujauddin Ahmmed, Arun Kumar Ray, Santanu Mondal

Abstract – **This paper proposes the design of 1.2-1.3 GHz, 2.5-3 GHz and 5.4-5.8 GHz MMIC voltage variable attenuator (VVA) realized using 0.25 μm GaAs pHEMT technology. It is a wideband voltage variable attenuator as it covers entire radar frequency bands. It provides a minimum attenuation of 2 dB in L and S-Band and 3 dB in C-Band and maximum attenuation of 72 dB in L-Band, 60 dB in S-Band and 47 dB in C-Band with attenuation flatness of 3 dB in L and S-Band and 1 dB in C-Band. The phase response of the attenuator is also shown in this paper. The attenuator is perfectly matched with source and load impedances. It shows full-band stability. By convention, noise figure is equal to attenuation. The novelty of this proposed design is source controlled attenuator using gm-reduction and double active termination techniques with noise figure less than attenuation. These techniques increase the dynamic range of attenuation and reduce noise figure also. The double active termination technique also contributes in reducing noise figure below each attenuation level. It is necessary to keep noise figure below attenuation because the attenuator will be used in RF front-end of radar receiver. By keeping noise figure below attenuation, sensitivity of radar receiver will improve. Input 1 dB compression point of the proposed attenuator at maximum attenuation are at -4.3 dBm in L-Band, -5.9 dBm in S-Band and -5.3 dBm in C-Band and OIP3 at minimum attenuation are at -4.4 dBm in L-Band, -4.6 dBm in S-Band and -5 dBm in C-Band. The ideal and post-layout simulation results are presented in this paper. Figure of merit of the proposed attenuator is 280 in L-Band, 70.3 in S-Band and 78.54 in C-Band. The attenuator can be used in single target tracking radar as well as in T/R module of AESA radar.**

Keywords – **Triple-band, Dynamic range, Insertion loss, MMIC, Noise figure, Source-controlled.**

I. INTRODUCTION

The voltage-variable attenuator provides variable attenuation depending on the control voltage applied. The prime objective of voltage variable attenuator is to control the signal strength [1]. An attenuator reduces input power by a predetermined ratio [2]. Recently pHEMT based attenuator is used in automatic gain control applications due to its capability of generating low noise. Voltage Variable Attenuator (VVA) is of two types-absorptive VVA and monolithic VVA. Source-controlled attenuator falls under the category of monolithic VVA. Although in Ref. [1], it is stated that impedance variation is the primary cause for the non-linear response of variable attenuators, we have leveraged this impedance variation to achieve high dynamic range of attenuation, low insertion loss and good linearity. Voltage variable attenuators can find applications in automatic gain control circuits in radar receivers. In case of target-tracking radar, signal-to-noise ratio increases when the target comes into radar's vicinity. This can cause the radar receiver to saturate. To prevent saturation of radar receiver, voltage variable attenuator is employed to attenuate the signal, enabling further processing by the receiver. The most common of the attenuators discussed in the literature are pi-type, T-type and cascaded pi-T type attenuator [3]. A negative feedback voltage variable attenuator described in [4] gives a bandwidth of 0.4 GHz in C-Band. The proposed design has better stability (> 5) compared to that of [4] which has stability >1. A variable attenuator designed in [5] gives an insertion loss of 6 dB and dynamic range of over 12 dB at 9-15 GHz frequency. Most of the attenuators mentioned in the literature are gate-controlled configuration. Ref. [8] shows the improvement of noise figure due to active termination. In the proposed design, gm-reduction technique and double active termination are used to get noise figure which is very less than attenuation. The attenuator is properly matched with source and load impedance. It is highly stable. The purpose of this paper is to mark the importance of source-controlled voltage variable attenuator, showing its inner working and shedding light on the practical applications. The proposed design is a source-controlled configuration with triple bandwidth, good linearity, high dynamic range of attenuation, low insertion loss and less noise figure as compared to attenuation. Section II describes the source-controlled attenuator. Section III highlights how dynamic range and noise figure is improved using gm-reduction method and double active termination technique. Section IV and V highlights layout and post-layout simulation results and its discussion. Section VI concludes the paper.

Article history: Received Month dd, yyyy; Accepted Month dd, yyyy

[1]Subham Banerjee, Md Sujauddin Ahmmed and Arun Kumar Ray are with the Integrated Test Range, Chandipur, India, E-mail: 9088983569subham@gmail.com, md.sujauddin@gmail.com, drakroy.itr@gov.in

Subham Banerjee and Santanu Mondal are with the Institute of Radio Physics & Electronics, Kolkata, India, E-mail: santanumondal2008@rediffmail.com

II. SOURCE-CONTROLLED ATTENUATOR

The MMIC layout is based on GaAs pHEMT technology using 0.25 μm pHEMT gate lengths. The MMICs are realized on substrate, with two thick gold metallization levels, thin film resistors, MESA resistor, MIM capacitors, spiral inductors and through the substrate via holes. The proposed circuit is miniature in size. This paper proposes the design of a

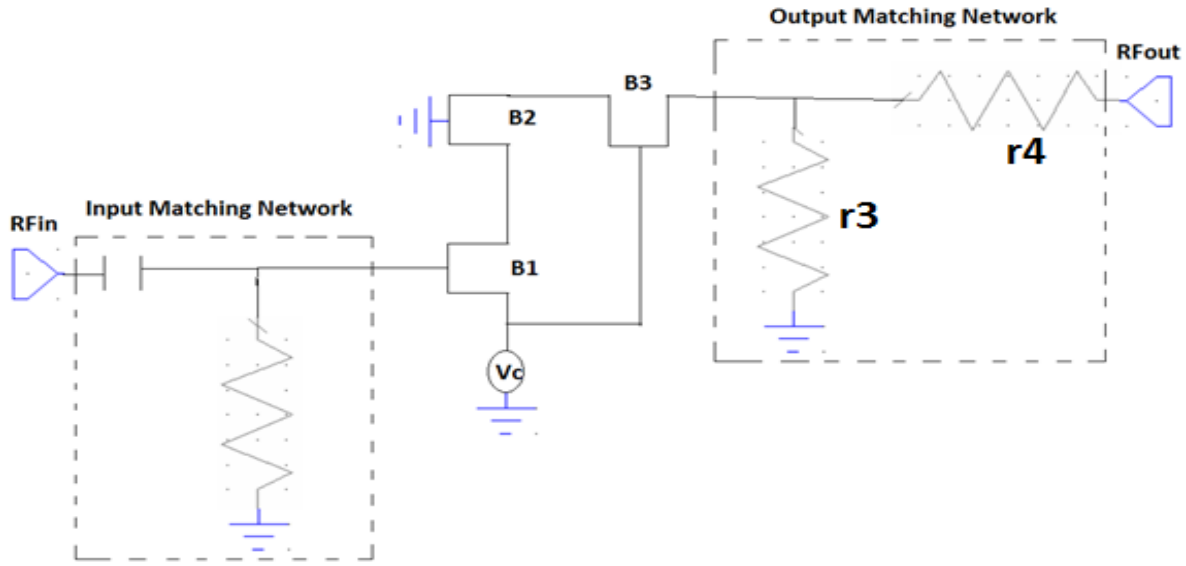

Fig. 1. Topology of triple-band attenuator

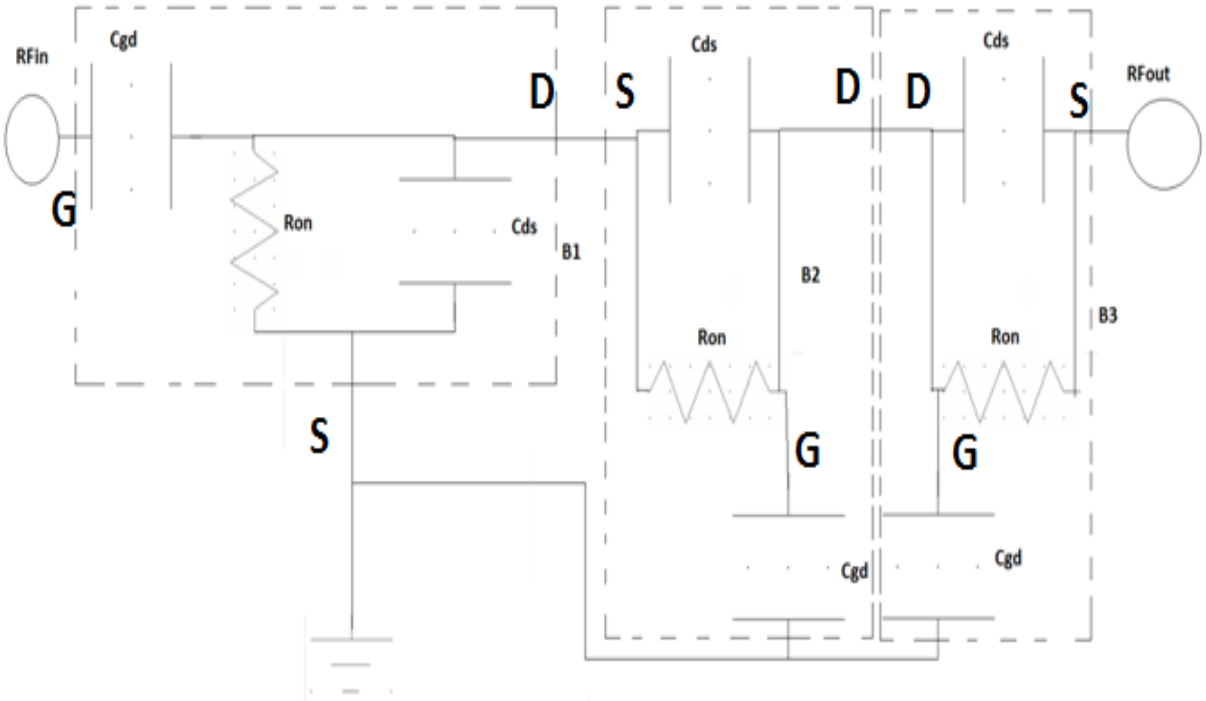

Fig. 2. pHEMT based equivalent circuit

1.2-1.3 GHz, 2.5-3 GHz and 5.4-5.8 GHz voltage variable attenuator (VVA) realized using 0.25 µm pHEMT. The post-layout simulation was carried out in Cadence AWR design environment. Figure 1 shows the proposed circuit diagram of L-, S- and C-Band attenuator. The operation of B1 is governed by the control voltage applied to the source terminal of B1 which increases the dynamic range of attenuation. The input and output matching networks are used to improve the input and output reflection coefficients respectively of the circuit. The internal parameters of the device are shown in Table 1 [6] [7].

TABLE 1
INTERNAL PARAMETERS OF PHEMT

Internal parameters	Values
R_{on}	7.6 Ω
Gate-to-drain capacitance (C_{gd})	0.87 fF
Drain-to-source capacitance (C_{ds})	28.5 fF

III. Dynamic Range and Noise Figure Improvement by Gm-Reduction and Double Active Termination Technique

A. Gm-Reduction Technique

The equivalent circuit [7] of the proposed attenuator is shown in Fig. 2. A GaAs MESFET or pHEMT is generally a field-controlled majority carrier device [2]. Here pHEMT operates by the field introduced by the control voltage applied to the source terminal of pHEMT. When control voltage is low (0.9 V), VGS is less negative and more than threshold voltage, the device B1 turns on and the source current reaches the load. When control voltage is high (2.2 V), VGS is highly negative and less than the threshold voltage, the device B1 turns off and there is no source current flowing through the circuit. The attenuation is given by Eq. (1).

$$A = g_{m,eq} Z_0, \tag{1}$$

where $g_{m,eq} = g_{m1} // g_{m2} // g_{m3}$ and g_{m1}, g_{m2} and g_{m3} are transconductances of $B1$, $B2$ and $B3$ respectively. The output impedance is given in Eq. (2).

$$Z = \frac{\frac{R_{on}}{\omega C_{ds}}}{\sqrt{\left(R_{on}^2\right) + \left(\left(\frac{1}{\omega C_{ds}}\right)^2\right)}}. \tag{2}$$

Here $Zo=Z_1+Z_2+Z_3$, Z_1, Z_2 and Z_3 are the output impedances of $B1$, $B2$ and $B3$ respectively. The transconductance of $B1$ depends on source current which in turn depends on source voltage i.e. control voltage. At maximum attenuation, transconductance is low as compared to minimum attenuation since source current is minimum at maximum attenuation. The transconductance decreases with increase in attenuation. Due to this gm reduction and double active termination [8] techniques, noise figure is less than attenuation at minimum and maximum attenuation. The equation for the minimum noise figure is given in [9].

$$F_{\min} = 1 + K_f \left(\frac{f}{f_T}\right) \sqrt{g_{meq}\left(R_g + R_s\right) + K_i}, \tag{3}$$

where R_g and R_s are the gate and source resistances of pHEMT. K_f and K_i are fukui constants, $g_{m,eq}$ is the overall transconductance, f is the operating frequency, f_T is the cutoff frequency. As transconductance decreases, minimum noise figure also decreases.

B. Double Active Termination Technique

The proposed double active termination technique has been adopted to improve noise figure performance.

Noise Voltage due to B2

It is formed by R_{on}-C_{ds} parallel source degeneration as shown in equivalent circuit of the attenuator. The attenuation can be expressed as:

$$A_{B2} \cong -\frac{g_{m2} R_l \left(1 + sR_{on}C_{ds}\right)}{1 + g_{m2}R_{on} + sR_{on}C_{ds}}, \tag{4}$$

where g_{m2} is transconductance of $B2$, R_l can be expressed as follows:

$$R_l = \left(\frac{\frac{R_{on}}{\left(\omega C_{ds}\right)^2}}{R_{on}^2 + \left(\frac{1}{\omega C_{ds}}\right)^2} + \frac{r_3\left(r_4 + 50\right)}{r_3 + r_4 + 50}\right) - j\left(\frac{R_{on}^2}{\omega C_{ds}\left(R_{on}^2 + \left(\frac{1}{\omega C_{ds}}\right)^2\right)}\right). \tag{5}$$

$r3$ and $r4$ are resistors of output matching network. The input-referred noise Power Spectral Density [8] contributed by $B2$ is calculated as follows:

$$\bar{V}_{n,in,B2}^2 = 4KT \frac{V_c^2 g_{m2} R_{o2}^2}{A_{B2}^2}. \tag{6}$$

R_{o2} is the output impedance of $B2$, V_c is the applied control voltage.

Noise Voltage due to B3

The attenuation due to B3 can be expressed as follows.

$$A_{B3} = -\frac{g_{m3} R_{l,B3}}{1 + g_{m3} R_{eq}}. \tag{7}$$

g_{m3} is the transconductance of $B3$, $R_{l,B3}$ and R_{eq} can be expressed as:

$$R_{l,B3} = \left(\frac{\frac{2R_{on}}{\left(\omega C_{ds}\right)^2}}{R_{on}^2 + \left(\frac{1}{\omega C_{ds}}\right)^2}\right) - j\left(\frac{2R_{on}^2}{\omega C_{ds}\left(R_{on}^2 + \left(\frac{1}{\omega C_{ds}}\right)^2\right)}\right), \tag{8}$$

$$R_{eq} = \frac{r_3\left(r_4 + 50\right)}{r_3 + r_4 + 50}. \tag{9}$$

The input-referred noise Power Spectral Density [8] contributed by $B3$ is calculated as follows:

$$\bar{V}_{n,in,B3}^2 = 4kT \frac{V_c^2 g_{m3} R_{o3}^2}{A_{B3}^2}. \tag{10}$$

R_{o3} is the output impedance of $B3$.

Total Noise Voltage

The total input-referred noise Power Spectral Density [8] contributed by $B2$ and $B3$ is calculated as follows.

$$NV_{total} = \bar{V}_{n,in,B2}^2 + \bar{V}_{n,in,B3}^2. \tag{11}$$

As per Fig. 6 of Section V, the noise figure is far below attenuation. It is due to g_m-reduction technique and double active termination technique. Double Active termination

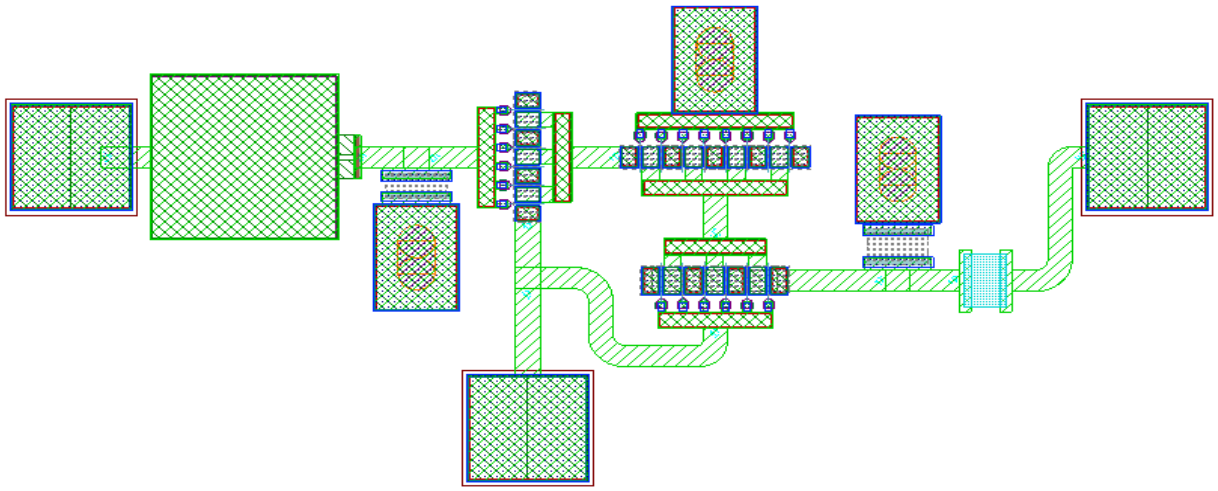

Fig. 3. Layout of the L, S and C-Band attenuator (layout size-979.2 µm x 442.3 µm)

technique reduces noise voltage more than the active termination technique.

IV. Layout and Post-Layout Simulation

The attenuator has been designed using WIN 0.25 µm pHEMT technology. In this process MIM capacitors, TFR and MESA resistors are available, which are used in this design. The layout occupies an area of 979.2 µm x 442.3 µm. The current consumption is maximum during minimum attenuation. The layout was carried out by connecting the lumped elements with the microstrip lines. Microstrip tee junction was used when there was a node connecting three branches. After layout, post-layout simulation was carried out and results are obtained. The post-layout simulation was carried out using 3D Axiem simulator. It was used for electromagnetic simulation of the microstrip lines. Electromagnetic simulation also considered the parasitic effects.

V. Results and Discussion

The transconductance decreases with increase in attenuation. During maximum attenuation, the transconductance is less as compared to the transconductance during minimum attenuation. Due to this g_m reduction technique and active termination[8], noise figure is less than attenuation at minimum and maximum attenuation. The plot of attenuation and noise figure against transconductance is shown in Fig. 4.

The transconductance decreases at maximum attenuation as shown in Fig. 4 and hence noise figure is less than or equal to attenuation. Fig. 5 shows that at each level of attenuation, noise figure is less than attenuation which is our primary requirement. In order to improve SNR and sensitivity of receiver, it is required to keep the noise figure below attenuation. The plot of attenuation and noise voltage with control voltage is shown in Fig. 6.

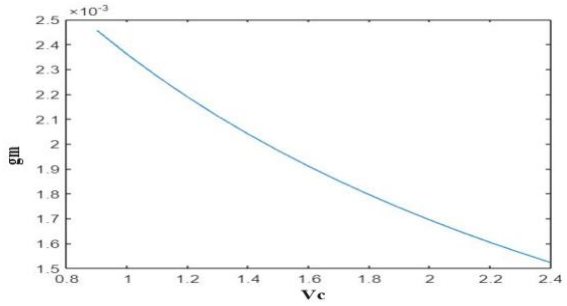

Fig. 4. Plot of transconductance with control voltage

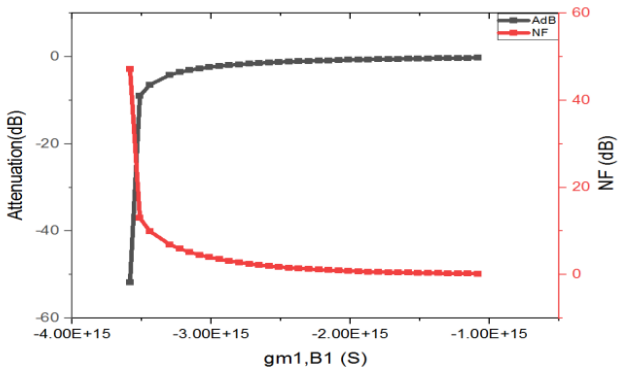

Fig. 5. Plot of attenuation and noise figure with transconductance

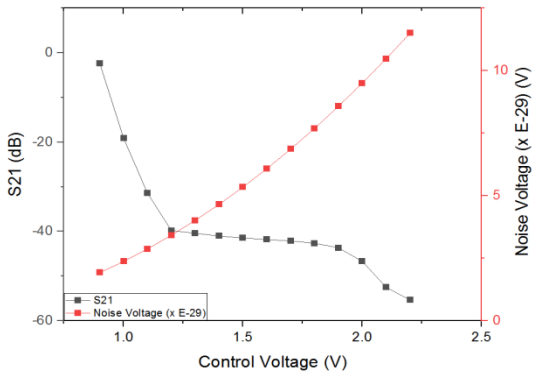

Fig. 6. Plot of attenuation and noise voltage with control voltage

As per Fig. 6, the noise figure is far below attenuation. It is due to g_m-reduction technique and double active termination technique. Double Active termination technique reduces noise voltage more than the active termination technique.

A. Minimum and Maximum Attenuation

The post-layout simulation results show that the performance of attenuator is undeviating from the ideal behavior. The novelty of the circuit is low insertion loss, high dynamic range of attenuation and less noise figure as compared to attenuation. In this section, V_c is an abbreviation for control voltage. The minimum attenuation is 2 dB. The S-curve of the attenuator follows the following path.

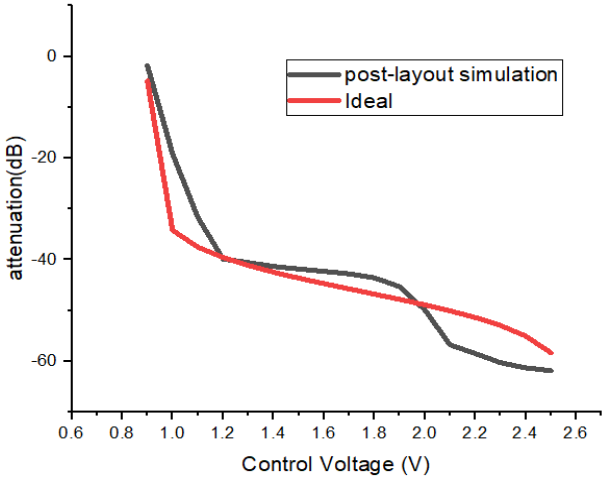

Fig. 7. Plot of attenuation with control voltage

The dynamic range of attenuation is approximately 70 dB in L-Band, 58 dB in S-Band and 44 dB in C-Band. The minimum attenuation of 2 dB occurs at a control voltage of 0.9 V in L and S Band and 3 dB in C-Band and maximum attenuation of 72 dB and 60 dB in L and S-Band and maximum attenuation of 47 dB in C-Band. The attenuation flatness is 3 dB in L, S-Band and 1 dB in C-Band.

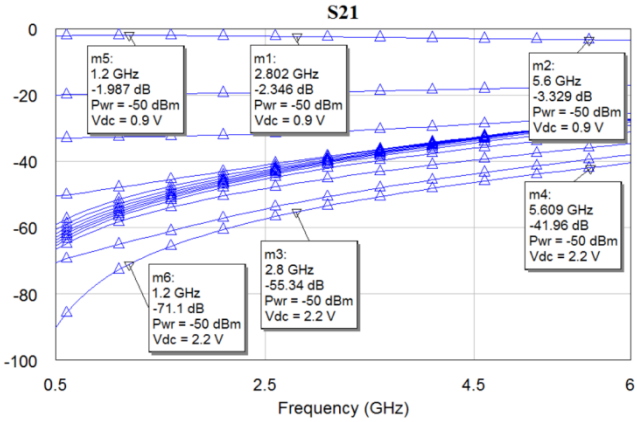

Fig. 8. Plot of attenuation of triple-band attenuator at control voltage ranging from 0.9 V to 2.2 V

The dynamic range of attenuation is approximately 70 dB in L-Band, 58 dB in S-Band and 44 dB in C-Band. The attenuation flatness are 3 dB in L and S-Band and 1 dB in C-Band. The phase of S_{21} with varying control voltage is shown in Fig. 9. The insertion phase variation are 1.7^0 in L-Band, 5^0 in S-Band and 4^0 in C-Band.

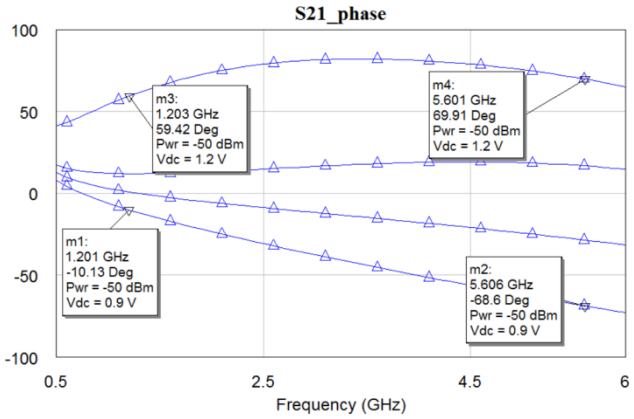

Fig. 9. Phase of S_{21} for varying control voltage

Input and output reflection coefficients are better than -10 dB. The input and output reflection coefficients at all the states are less than -10 dB. Fig. 10 shows the plot of reflection coefficients in the required frequency bands. The proposed attenuator is a triple-band design where S_{11} and S_{22} are much below -10 dB in the required frequency band.

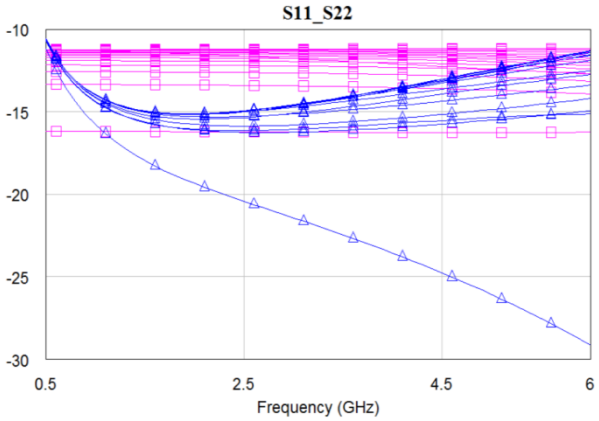

Fig. 10. Input and output reflection coefficients of the triple-band attenuator at control voltage ranging from 0.9 V to 2.2 V (blue-S_{11} and pink-S_{22})

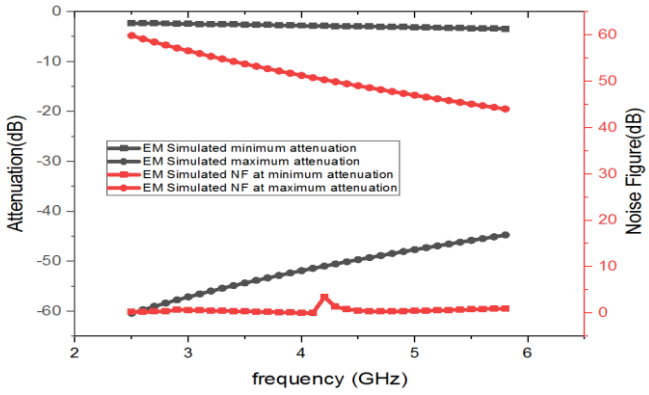

Fig. 11. Plot of attenuation and noise figure at minimum and maximum attenuation

As the voltage variable attenuator will be used in front-end of radar receiver along with Low Noise Amplifier, it is important to keep the noise figure below attenuation. By doing so, sensitivity of receiver will improve. The noise figure corresponding to minimum attenuation of 2 dB is 0.01 dB in L-Band, 0.2 dB in S-Band whereas in C-Band, it is 0.6 dB which corresponds to a minimum attenuation of 3 dB. Similarly, at maximum attenuation, noise figure is less than or equal to attenuation as shown in Fig. 11.

B. Group Delay

The proposed attenuator gives a group delay of less than 0.1 ns across 0.1 GHz span in 1.2-1.3 GHz, 2.5-3 GHz and 5.4-5.8 GHz (Fig. 12). The group delay variation is less than 0.1 ns at minimum and maximum attenuation levels.

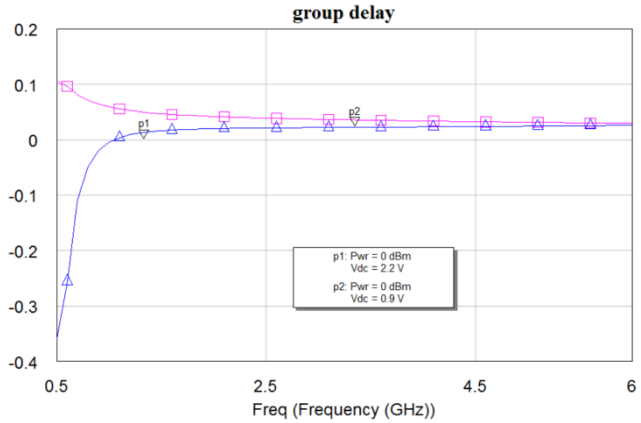

Fig. 12. Group delay variation at minimum and maximum attenuation

C. Stability Analysis

The proposed design is stable across 0.1 GHz span in 1.2-1.3 GHz, 2.5-3 GHz and 5.4-5.8 GHz at all values of control voltage (Fig. 13). At control voltage of 0.9 V, the stability factor (k-value) at 2.8 GHz is greater than 9 and at 5.6 GHz it is greater than 6. At other control voltages, the stability factor (k-value) is higher than 10.

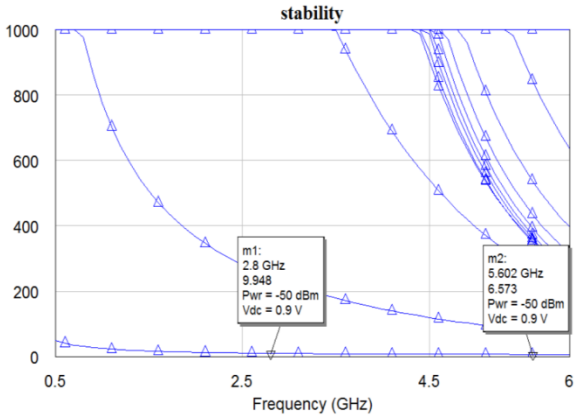

Fig. 13. Plot of stability factor (k-value) with frequency for different values of control voltage

D. Linearity Analysis

Two important parameters for determining linearity of a circuit are 1 dB compression point and input intercept point of order 3 (Fig. 14). At maximum attenuation, input 1 dB compression point are at -4.3 dBm in L-Band, -5.9 dBm in S-Band and -5.3 dBm in C-Band and OIP3 (Fig. 15) at minimum attenuation are at -4.4 dBm in L-Band, -4.6 dBm in S-Band and -5 dBm in C-Band.

The proposed attenuator shows relatively better performance than previous mentioned works. The proposed attenuator can be used in ground station radar, operating in L-Band, S-Band and C-Band for effectively tracking of the target. The source-controlled attenuator gives low insertion loss, high dynamic range of attenuation and less noise figure as compared to attenuation which is not present in the literature. Though the dynamic range is very high, up to 30 dB of maximum attenuation is considered because in this range, the phase of S_{21} varies between -50^0 to $+50^0$. FOM of the proposed attenuator is 280 in L-Band, 70.3 in S-Band and 75.84 in C-Band. Table 2 shows the performance comparison of the proposed design with the other works in the literature. The proposed design outperforms the performance of the existing gate-controlled attenuator in the literature as shown in Table 2.

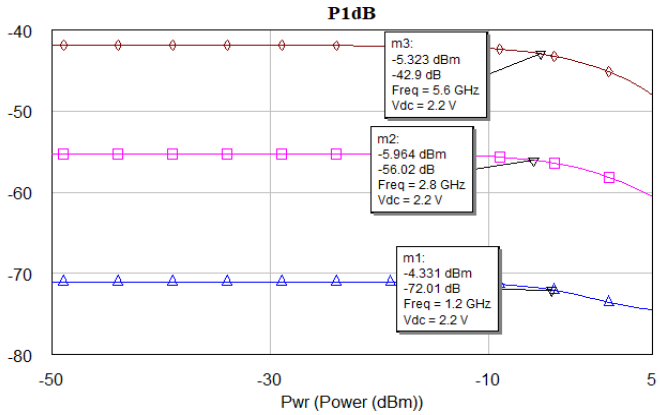

Fig. 14. Plot of 1 dB compression point of the proposed triple-band attenuator

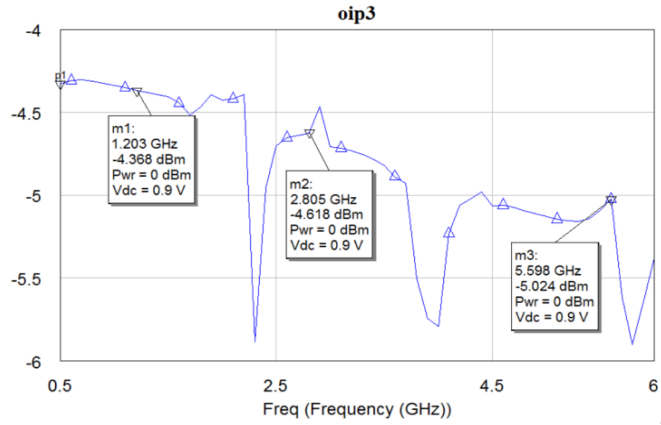

Fig. 15. Plot of OIP3 of the proposed triple-band attenuator

VI. CONCLUSION

The proposed design gives a large dynamic range with less noise figure as compared to attenuation, low insertion loss and good linearity. The total occupied area was about 0.4312 mm2 and the current consumption was about 8 mA during minimum attenuation. Dynamic range is enhanced and noise figure is greatly reduced by applying the method of gm-reduction and double active termination techniques. The dynamic range of attenuation achieved was about 70 dB and input and output reflection coefficients were less than -10 dB for entire range of control voltage. The OIP3 was found to be -4.4 dBm in L-Band, -4.6 dBm in S-Band and -5 dBm in C-Band. Though the dynamic range is very high, we will consider up to 30 dB because in this range, the phase of S21 varies between -500 to +500. Characterizing with large dynamic range, miniature size, low insertion loss and less noise figure as compared to attenuation, the attenuator can be used in single target tracking radar and T/R module of AESA radar.

TABLE 2
COMPARISON OF SOURCE-CONTROLLED ATTENUATOR WITH THE EXISTING GATE-CONTROLLED ATTENUATOR

Ref.	Topology	Frequency	Minimum attenuation	Maximum attenuation	Reflection coefficient	Area	Noise Figure	FOM
[10]	Local feedback	26-30 GHz	N/A	Attenuation Range-18 dB	N/A	N/A	-	-
[11]	-	10-14.4 GHz	N/A	Attenuation range-22 dB	< -11	0.7 mm^2	-	-
[12]	Switched path and T w/ active switch	2-20 GHz	N/A	Attenuation range-31.5 dB	< -9	1.725 mm^2	-	-
[13]	-	0.06 GHz	N/A	Attenuation range-48 dB	N/A	0.1 mm^2	-	-
[14]	-	DC-3.7 GHz	0.9-1.25	~37 dB	< -10.6 dB	0.27 mm^2	-	1.42
[15]	-	0.4-3.7 GHz	2.1 dB	33 dB	< -9 dB	-	-	25.35
This work	1 Stage attenuator with gm-reduction and double active termination	1.2-1.3 GHz, 2.5-3 GHz & 5.4-5.8 GHz	2 dB & 3 dB	72 dB, 60 dB & 47 dB	<< -10 dB	0.4312 mm^2	<= attenuation	280 in L-Band, 70.3 in S-Band and 78.54 in C-Band

ACKNOWLEDGEMENT

The work is supported by Integrated Test Range and University of Calcutta. I like to thank Director of Integrated Test Range, Shri H. K. Ratha, Additional Director of Radar Division, Dr. Niladri Roy and Group Director of Radar Division, Shri N. Biswal for providing me the opportunity to do this work.

REFERENCES

[1] Y.-Y. Huang, W. Woo, Y. Yoon and C.-H. Lee, "Highly Linear RF CMOS Variable Attenuators With Adaptive Body Biasing," in *IEEE Journal of Solid-State Circuits*, vol. 46, no. 5, pp. 1023-1033, May 2011.

[2] B. Maoz, "A novel, linear voltage variable MMIC attenuator, " in *IEEE Transactions on Microwave Theory and Techniques*, vol. 38, no. 11, pp. 1675-1683, Nov. 1990.

[3] W. Cheng, M. S. Oude Alink, A. J. Annema, G. J. M. Wienk and B. Nauta, "A Wideband IM3 Cancellation Technique for CMOS Π- and T-Attenuators," in *IEEE Journal of Solid-State Circuits*, vol. 48, no. 2, pp. 358-368, Feb. 2013.

[4] M. S. Ahmmed, S. Banerjee, A. K. Ray and R. K. Chaudhury, "Design of MMIC Voltage Variable Attenuator for T/R Module of Phased Array Radar, " *2nd International Conference on Range Technology (ICORT)*, Chandipur, Balasore, India, 2021, pp. 1-4,

[5] R. Teja N., P. Verma, A. Kumar and A. N. Bhattacharya, "A Dual-Band High Linearity Voltage Variable Attenuator MMIC," *6th International Conference on Computers and Devices for Communication (CODEC)*, Kolkata, India, 2015, pp. 1-4.

[6] N. R. Das, P. K. Basu and M. J. Deen, "A New Approach to the Design Optimization of HEMT and HBT for Maximum Gain-Bandwidth of MSM-Based Integrated Photoreceiver and its Noise Performance at 1.55 /spl mu/m," in *IEEE Transactions on Electron Devices*, vol. 47, no. 11, pp. 2101-2109, Nov. 2000.

[7] Z. Hu, S. Zhou, R. He and Q. Zhang, "A Dual-band Voltage Variable Attenuator With High-Power Tolerance and Compact Size Based on Dual-Gate GaN HEMTs," in *IEEE Transactions on Power Electronics*, vol. 38, no. 5, pp. 6108-6115, May 2023.

[8] X. Yan, H. Luo, J. Zhang, H. Zhang and Y. Guo, "Design and Analysis of a Cascode Distributed LNA With Gain and Noise Improvement in 0.15-μm GaAs pHEMT Technology, " in *IEEE Transactions on Circuits and Systems II: Express Briefs*, vol. 69, no. 12, pp. 4659-4663, Dec. 2022.

[9] H.-S. Yoon, J.-H. Lee, B.-S. Park, C.-E. Yun and C.-S. Park, "Fabrication and Characteristics of Extremely Low-Noise AlGaAs/InGaAs/GaAs Pseudomorphic Hemts, " in *Journal of the Korean Physical Society*, vol. 33, no. 6, pp. 741-744, December 1998.

[10] B. Sadhu, J. F. Bulzacchelli, A. Valdes-Garcia, "A 28GHz SiGe BiCMOS Phase Invariant VGA", *IEEE Radio Frequency Integrated Circuits Symposium (RFIC)*, San Francisco, CA, USA, 2016, pp. 150–153.

[11] F. Padovan, M. Tiebout, A. Neviani, A. Bevilacqua, "A 12 GHz 22 dB-Gain-Control SiGe Bipolar VGA with 2° Phase-Shift Variation", in *IEEE Journal of Solid-State Circuits*, vol. 51(7), pp. 1525-1536, July 2016.

[12] M.-K. Cho; I. Song; Z. E. Fleetwood, J. D. Cressler, "A SiGe-BiCMOS Wideband Active Bidirectional Digital Step Attenuator With Bandwidth Tuning and Equalization", in *IEEE Trans Microwave Theory Tech*., vol. 66, pp. 3866 – 3876, 2018.

[13] S.-Y. Kang, S.-T. Ryu, C.-S. Park , "A Precise Decibel-Linear Programmable Gain Amplifier Using a Constant Current-Density Function", in *IEEE Trans Microwave Theory Tech*., vol. 60, pp. 2843-2850 2012.

[14] Li D, Fei C, Li Y, Zhang Q, Yang Y. "A Large Dynamic Range Voltage Controlled Attenuator with Improved Linearity-in-db for Ultrasound Applications", in *International Journal of Circuit Theory and Applications*, pp. 1–15, 2019.

[15] Y.-Y. Huang, W. Woo, Y. Yoon, C.-H. Lee, "Highly linear RF CMOS Variable Attenuators With Adaptive Body Biasing", in *IEEE Journal of Solid-State Circuits*,vol. 46, pp. 1023-1033, 2011.